Evolution of transmitted depolarization in diffusely scattering media

THOMAS A. GERMER[1,*]

[1] *Sensor Science Division, National Institute of Standards and Technology, Gaithersburg, Maryland 20899, USA*
[*] *thomas.germer@nist.gov*

Abstract: We performed Mueller matrix Monte Carlo simulations of the propagation of optical radiation in diffusely scattering media for collimated incidence and report the results as a function of thickness and the angle subtended by the detector. For sufficiently small thickness, a fraction of the radiation does not undergo any scattering events and is emitted at zero angle. Thus, for a very small detector angle, the measured signal will mostly indicate the attenuation of the coherent contribution, while for larger angles, the diffuse scattering radiation will contribute significantly more. The degree to which the radiation is depolarized thus depends on the angle subtended by the detector. A three-stream model, where the coherent radiation, the forward diffusely scattered radiation, and the backward scattered radiation are propagated according to the differential Mueller matrix formalism is introduced and describes the results from the Monte Carlo simulations and the results of measurements well. This scatter-based model for depolarization in diffusely scattering media is an alternative to that based upon elementary fluctuation theory applied to a single propagation stream. Results for average photon path length, determined from the Monte Carlo simulations, suggest that applying fluctuation theory to photon path length may unify the two approaches.

1. Introduction

The evolution of depolarization of optical radiation as it transmits through diffusely scattering media is of interest in a number of applications, including biomedical imaging [1], remote sensing [2–4], material characterization [5], and optical devices [6]. In general, depolarization results from a random variable that is encountered in the numerous paths that radiation takes in propagating from a source to a detector. In many cases, the onset of depolarization has been found to be quadratic with material thickness [7–9], while in others, the observed behavior has been more complicated [10, 11].

The evolution of the intensity and polarization state of radiation transmitting through a medium is often treated in terms of a 4×4 Mueller matrix $\mathbf{M}(z)$ that evolves according to the differential equation [12–14]

$$\frac{\mathrm{d}\mathbf{M}(z)}{\mathrm{d}z} = \mathbf{m}(z)\mathbf{M}(z), \tag{1}$$

with the initial condition $\mathbf{M}(0) = \mathbf{I}$ (the identity matrix), where $\mathbf{m}$ is a 4×4 differential Mueller matrix, and z is the propagation coordinate. When $\mathbf{m}$ is independent of z, the solution for a layer of thickness Δz is well known:

$$\mathbf{M}(\Delta z) = \exp(\mathbf{m}\Delta z), \tag{2}$$

where the matrix exponential is used [15]. The behavior described by Eq. (2) motivates the logarithmic decomposition of a Mueller matrix [16, 17],

$$\mathbf{L} = \log(\mathbf{M}/M_{00}). \tag{3}$$

One model for depolarization of the radiation is to consider fluctuations in the matrix $\mathbf{m}$. In this case, if the material is longitudinally homogeneous (long correlation length limit), the

logarithmic decomposition is approximately given by [18, 19]

$$\mathbf{L} = \langle \mathbf{m} \rangle \Delta z + \frac{1}{2} \langle \Delta \mathbf{m}^2 \rangle \Delta z^2, \tag{4}$$

while for short Gaussian correlation lengths $z_g \ll \Delta z$,

$$\mathbf{L} = \langle \mathbf{m} \rangle \Delta z + \frac{1}{2} \langle \Delta \mathbf{m}^2 \rangle (\pi^{1/2} z_g \Delta z - z_g^2). \tag{5}$$

A brief derivation of Eqs. (4) and (5) is given in the Appendix. The matrix $\langle \mathbf{m} \rangle$ is non-depolarizing, while the variance $\langle \Delta \mathbf{m}^2 \rangle$ is depolarizing.

Several studies have observed quadratic evolution of depolarization, at least for small thicknesses [7–10], and have attributed that behavior to the application of Eq. (4). However, in a number of these studies [7, 8, 10], the assumption of longitudinal homogeneity should not have applied. In Refs. [7] and [8], layers of independent materials were stacked to vary the thickness. Since these layers were solid, the fluctuations of their optical properties would have been stationary, and no correlations between layers should have existed. Within the fluctuation theory, if each layer of thickness z_0 is homogeneous along the propagation direction, the Mueller matrix of n independent layers (i.e., long correlation within a layer, but no correlation between layers) would be

$$\mathbf{M} = \exp\left(n \langle \mathbf{m} \rangle z_0 + \frac{n}{2} \langle \Delta \mathbf{m}^2 \rangle z_0^2 \right). \tag{6}$$

That is, if the fluctuation theory described the origin of depolarization in the layered samples, the growth of depolarization would have been linear with the number of layers.

The problem with applying Eq. (1) to the propagation of radiation through a diffusely scattering medium is that the radiation is not propagating in a single direction. The path lengths take on a distribution with a mean length significantly greater than the material thickness [20–23]. Furthermore, if one were to add independent layers, the presence of an additional layer affects the field distribution in previous layers.

We previously proposed an alternative approach to understanding the evolution of depolarization [24], introducing a two-stream model, where radiation can propagate not only forward, but also backward through the media. This is a crude approximation to the radiative transfer equation, where there is a continuum of propagation directions, but it serves the purpose of demonstrating that, by simply allowing radiation to propagate in multiple directions and having the only depolarizing mechanism be in the scattering matrix elements, quadratic evolution of depolarization naturally occurred. The evolution becomes linear for sufficiently large thicknesses, much as the fluctuation theory does.

Charbois and Devlaminck published results for depolarization for emulsions as a function of thickness, showing markedly non-quadratic behavior [10]. In some cases, the initial evolution was cubic, in some there appeared to be an incubation length before any depolarization was observed at all, and still others the behavior exhibited weak oscillations. The measurements showing non-quadratic evolution used a very small collection angle ($\beta = 0.6°$). When radiation was collection over a larger angle using a lens, the evolution appeared more quadratic. These measurements were published along with a generalized fluctuation theory that handled the case of partial correlation length. While they achieved reasonable fits of their theory to their data, they acknowledged that they had no physical understanding for what some of those results represented. Non-quadratic results were also obtained by Gompf *et al.*, whose instrument also has a very small collection angle [11].

In this article, we extend the scattering approach by performing Monte Carlo (MC) simulations and considering the Mueller matrix for different angles subtended by the detector. The measurement geometry is described schematically in Fig. 1. If we assume that there is no depolarization except that which occurs through scattering, we can replicate the complicated

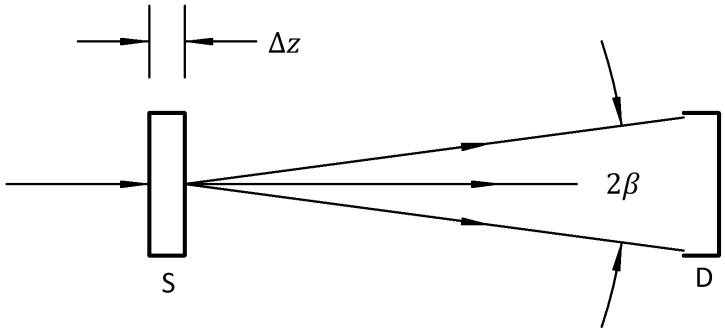

Fig. 1. The virtual measurement setup. Collimated radiation strikes material S of thickness Δz and radiation emitted from the material with angles within 2β is collected by detector D.

behavior observed in Charbois and Devlaminck's measurements. The unscattered radiation, which dominates the signal for a small collection angle and small thicknesses, exhibits no depolarization. Thus, appreciable depolarization does not occur until the unscattered beam is attenuated to a level comparable to the diffusely scattered radiation.

We start by describing the MC simulations in Sec. 2. In Sec. 3, we review the two-stream model originally presented in [24], deriving analytic expressions for isotropic media. We then introduce a three-stream model in Sec. 4, where the third stream represents the unscattered radiation. In Sec. 5, we present the results. The three-stream results fit the MC simulated data well. While data that evolves quadratically can be interpreted in light of the two-stream model, we believe the more complicated behavior observed by Charbois and Devlaminck can be understood with this three-stream scattering approach. We present path length results and suggest that the resolution to the discrepancy between the single-stream fluctuation theory and the scattering approach lies in the interpretation of the propagation coordinate in the former. We summarize our results in Sec. 6.

2. Monte Carlo Modeling

Single scattering phase functions (the normalized scattering probability as functions of angle θ) required for MC simulations were determined by obtaining the average Mueller matrix differential scattering cross section for a log-normal distribution (characterized by mean diameter D_0 and logarithmic width $\Delta D/D_0$) of spherical particles (index of refraction $n_{\text{sph}} = 1.56$) in water (index of refraction $n_{\text{water}} = 1.33$) using Mie theory with a wavelength of 532 nm and with 10^4 particles. The phase functions were tabulated in 1° steps, constituting an interpolation table. Three different phase functions were used, that associated with Rayleigh scattering (limit of small D_0) and those associated with mean diameters D_0 of 250 nm and 700 nm. The distribution width was fixed to $\Delta D/D_0 = 0.5$. Figure 2 shows the unique, non-zero elements of these phase functions in the local single scattering basis.

A ray propagating in the medium is assumed to have a mean scattering rate μ_{s}, which is fixed in this paper to $\mu_{\text{s}} = 1$ (which defines the length scale for thickness Δz). The distance between scattering events is randomly selected from an exponentially-distributed random number generator. At each scattering event, a new random direction is selected from the previous direction with a probability determined by the unpolarized part of the normalized phase function and with a uniform azimuth. Each ray carries with it its direction, position, and net Mueller matrix, which after the n-th scattering interaction is

$$\mathbf{M}_n = \mathbf{R}_b \mathbf{M}_{\text{pf}} \mathbf{R}_a \mathbf{M}_{n-1}, \tag{7}$$

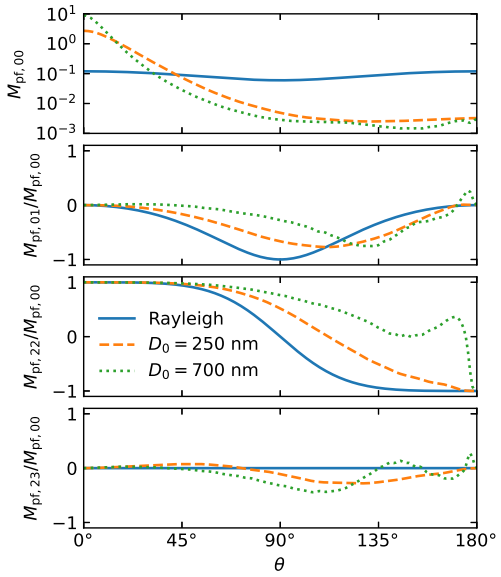

Fig. 2. The unique, non-zero elements of the Mueller matrix phase function $\mathbf{M}_{\text{pf}}$ for the three different particle size distributions used in the simulations.

where $\mathbf{M}_{n-1}$ is the accumulated Mueller matrix for the previous $n-1$ scattering events, $\mathbf{R}_a$ is a matrix that rotates the global polarization basis into the local polarization basis, $\mathbf{M}_{\text{pf}}$ is the normalized Mueller matrix phase function, and $\mathbf{R}_b$ is a matrix that rotates the local polarization basis to the global polarization basis. The starting Mueller matrix $\mathbf{M}_0 = \mathbf{I}$. The global polarization basis is one that does not have any singularities at the surface normal, so that it will be smoothly varying across the virtual detector. The local polarization basis is that parallel and perpendicular to the plane containing the incident and scattering rays for each scattering event.

Any ray that reaches the material boundary before its next scattering event is assumed to escape and, if its direction is within the right circular cone subtended by half angle β along the transmitted surface normal, accumulated to obtain the net Mueller matrix. For these simulations, we considered $\beta = 1°$, $5°$, or $20°$. For most of the simulations, 24×10^7 rays were propagated for each data point. This large number of rays was necessary, because most rays that have undergone scattering are lost, especially in the smallest of the detectors.

For simplicity, we have ignored interface reflections as well as refraction at the entrance and exit of the medium. Transmission and reflection can be polarization dependent, especially at large angles, but it is believed that the two interfaces of the liquid medium (as well as any container interfaces) have negligible effect on the polarization, compared to the diffuse scattering that occurs in the medium. Furthermore, no absorption, either in the medium surrounding the particles, nor in the particles themselves, was included. The lack of the inclusion of refraction would suggest that the actual collection angles in air would correspond to 1.33°, 6.66°, and 27.1°, respectively, by Snell's law.

3. Two-Stream Approach

In this section, we outline the theory originally described in [24]. When ignoring sample birefringence and including only diagonal depolarization, we can derive analytic expressions for the depolarization. The approach we take is a polarimetric extension of the theory of Kubelka and Munk (KM) (originally developed for reflectance, but applied here in transmittance) and

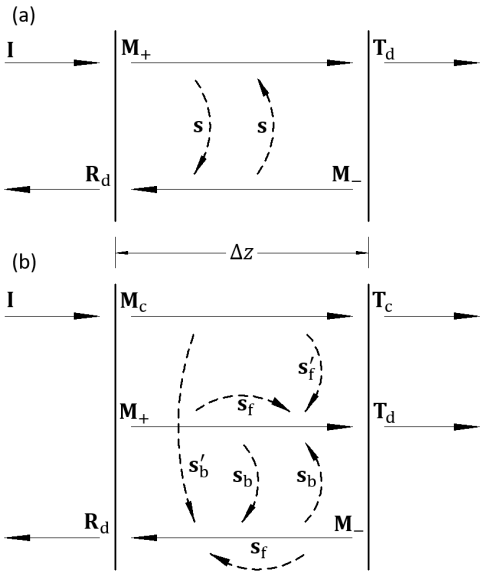

Fig. 3. Schematics of the (a) two-stream approach and (b) the three stream approach. Horizontal arrows indicate Mueller matrix streams, and dashed curves indicate scattering elements coupling the streams.

represents the simplest approximation to the radiative transfer equation [25, 26].

We begin by assuming that there are two streams, one propagating forward and one propagating backward, and that there is coupling between the two due to scattering. Figure 3(a) shows a schematic of this two stream model. Following KM, but generalizing the absorption and scattering coefficients with matrices, we have

$$\frac{\mathrm{d}}{\mathrm{d}z}\begin{pmatrix}\mathbf{M}_+(z)\\ \mathbf{M}_-(z)\end{pmatrix} = \mathbf{m}'\begin{pmatrix}\mathbf{M}_+(z)\\ \mathbf{M}_-(z)\end{pmatrix}, \tag{8}$$

where

$$\mathbf{m}' = \begin{pmatrix}\mathbf{m}-\mathbf{a}(\mathbf{s}) & \mathbf{r}(\mathbf{s})\\ -\mathbf{s} & \mathbf{r}[\mathbf{a}(\mathbf{s})-\mathbf{m}]\end{pmatrix}, \tag{9}$$

$\mathbf{m}$ is the forward differential Mueller matrix [as for Eq. (1)], and $\mathbf{s}$ is a scattering Mueller matrix. The matrices $\mathbf{M}_+(z)$ and $\mathbf{M}_-(z)$ represent the Mueller matrices for forward and backward propagating radiation, respectively. The matrix function $\mathbf{a}(\mathbf{s})$ is needed to account for polarization-dependent losses in one direction as radiation is scattered into the other, and is a non-depolarizing, diattenuative, and lossy differential Mueller matrix:

$$\mathbf{a}(\mathbf{s}) = \begin{pmatrix} s_{00} & s_{01} & s_{02} & s_{03}\\ s_{01} & s_{00} & 0 & 0\\ s_{02} & 0 & s_{00} & 0\\ s_{03} & 0 & 0 & s_{00}\end{pmatrix}. \tag{10}$$

The matrix function $\mathbf{r}(\mathbf{m})$ relates the forward propagating optical properties to the backward propagating ones that result from the use of different coordinate systems for propagation in each

direction [27]:

$$\mathbf{r}(\mathbf{m}) = \begin{pmatrix} m_{00} & m_{01} & -m_{02} & m_{03} \\ m_{10} & m_{11} & m_{12} & -m_{13} \\ -m_{20} & m_{21} & m_{22} & m_{23} \\ m_{30} & -m_{31} & m_{32} & m_{33} \end{pmatrix}. \tag{11}$$

The solution to Eq. (8) is

$$\begin{pmatrix} \mathbf{M}_+(z) \\ \mathbf{M}_-(z) \end{pmatrix} = \exp(\mathbf{m}'z) \begin{pmatrix} \mathbf{M}_+(0) \\ \mathbf{M}_-(0) \end{pmatrix}, \tag{12}$$

and we apply the boundary conditions

$$\begin{pmatrix} \mathbf{M}_+(0) \\ \mathbf{M}_-(0) \end{pmatrix} = \begin{pmatrix} \mathbf{I} \\ \mathbf{R}_\mathrm{d} \end{pmatrix}, \tag{13}$$

$$\begin{pmatrix} \mathbf{M}_+(\Delta z) \\ \mathbf{M}_-(\Delta z) \end{pmatrix} = \begin{pmatrix} \mathbf{T}_\mathrm{d} \\ \mathbf{0} \end{pmatrix}, \tag{14}$$

where $\mathbf{R}_\mathrm{d}$ is the Mueller matrix diffuse reflectance, and $\mathbf{T}_\mathrm{d}$ is the Mueller matrix diffuse transmittance. Reflectance and transmittance at the $z = 0$ and $z = \Delta z$ interfaces can be included with other boundary conditions but are not included here for simplicity.

If the material is isotropic and non-absorbing, the forward matrix is $\mathbf{m} = \mathbf{0}$, and

$$\mathbf{s} = \mathrm{diag}(s_0, s_1, -s_1, s_3). \tag{15}$$

It helps to let $\mathbf{m}$ have a small isotropic absorbing contribution, and then, after the matrix exponential is performed, to take the limit as that absorption vanishes. Because its submatrices are diagonal, the 8×8 matrix in Eq. (9) reduces to four 2×2 matrices of the form

$$\begin{pmatrix} -s_0 & s_j \\ -s_j & s_0 \end{pmatrix}. \tag{16}$$

The solution to Eqs. (8) through (14) is found to be

$$T_{\mathrm{d},00} = 1/(1 + s_0\Delta z), \tag{17}$$

$$R_{\mathrm{d},00} = s_0\Delta z/(1 + s_0\Delta z), \tag{18}$$

$$T_{\mathrm{d},jj} = \frac{P_j}{P_j \cosh(P_j\Delta z) + s_0 \sinh(P_j\Delta z)}, \tag{19}$$

$$R_{\mathrm{d},jj} = \frac{s_j}{s_0 + P_j \coth(P_j\Delta z)}, \tag{20}$$

where $P_j = (s_0^2 - s_j^2)^{1/2}$. The off-diagonal ($j \neq k$) elements $T_{\mathrm{d},jk}$ and $R_{\mathrm{d},jk}$ are zero. The logarithmic decomposition of the Mueller matrix transmittance is $L_{jj} = \log(T_{\mathrm{d},jj}/T_{\mathrm{d},00})$ and can be power series expanded to yield

$$L_{jj} = -\frac{1}{2}P_j^2(\Delta z)^2 + \frac{1}{3}s_0P_j^2(\Delta z)^3. \tag{21}$$

Note that for Δz much less than the scattering length $1/s_0$, the behavior is quadratic. When Δz approaches that length, significant higher order terms lead to a nearly linear behavior, approaching a slope of $-P_j$:

$$L_{jj} = -P_j \Delta z + \log\left[\Delta z\left(2s_0 - 2\frac{s_0^3}{s_j^2} + 2\frac{s_0^2 P_j}{s_j^2}\right)\right]. \tag{22}$$

Multiple scattering is the root of why depolarization behaves quadratically in this model. In order for scattering to affect radiation in transmission, there must be at least two scattering events: one to transfer radiation from the forward direction to the backward direction, and a second to transfer radiation back to the forward direction.

4. Three-Stream Approach

While the two stream approach given above in Sec. 3 may be sufficient for many applications, our MC results suggest that, at least in some cases, the coherent contribution must be treated separately in order to understand the results. In this section, we will describe a simple three-stream approach for modeling diffuse scatter in turbid media. We expand the two-stream model by distinguishing between radiation that has undergone scattering from that which has not. Thus, we consider three streams: a coherent stream in the forward direction and forward and backward diffuse streams. Radiation in the coherent stream can be lost to absorption, can undergo retardance and diattenuation, and be lost to the other streams due to scattering. However, we assume that radiation which has been scattered from the diffuse streams does not flow back to the coherent stream. Figure 3(b) is a schematic of the model. The differential equation governing this system is

$$\frac{\mathrm{d}}{\mathrm{d}z}\begin{pmatrix} \mathbf{M}_\mathrm{c}(z) \\ \mathbf{M}_+(z) \\ \mathbf{M}_-(z) \end{pmatrix} = \begin{pmatrix} \mathbf{m} - \mathbf{a}(\mathbf{s}'_\mathrm{f} + \mathbf{s}'_\mathrm{b}) & \mathbf{0} & \mathbf{0} \\ \mathbf{s}'_\mathrm{f} & \mathbf{m} - \mathbf{a}(\mathbf{s}_\mathrm{b} + \mathbf{s}_\mathrm{f}) + \mathbf{s}_\mathrm{f} & \mathbf{r}(\mathbf{s}_\mathrm{b}) \\ -\mathbf{s}'_\mathrm{b} & -\mathbf{s}_\mathrm{b} & -\mathbf{r}[\mathbf{m} - \mathbf{a}(\mathbf{s}_\mathrm{b} + \mathbf{s}_\mathrm{f}) + \mathbf{s}_\mathrm{f}] \end{pmatrix}\begin{pmatrix} \mathbf{M}_\mathrm{c}(z) \\ \mathbf{M}_+(z) \\ \mathbf{M}_-(z) \end{pmatrix}, \tag{23}$$

where $\mathbf{s}_\mathrm{f}$ and $\mathbf{s}_\mathrm{b}$ are forward and backward scattering Mueller matrices between the diffuse streams, respectively, while $\mathbf{s}'_\mathrm{f}$ and $\mathbf{s}'_\mathrm{b}$ are forward and backward scattering Mueller matrices from the coherent stream to the diffuse streams, respectively. The matrix $\mathbf{M}_\mathrm{c}$ represents the Mueller matrix for the coherent stream, while the matrices $\mathbf{M}_+(z)$ and $\mathbf{M}_-(z)$ represent the Mueller matrices for forward and backward propagating diffuse radiation, respectively. Eq. (23) needs to be solved under the boundary conditions

$$\begin{pmatrix} \mathbf{M}_\mathrm{c}(0) \\ \mathbf{M}_+(0) \\ \mathbf{M}_-(0) \end{pmatrix} = \begin{pmatrix} \mathbf{I} \\ \mathbf{0} \\ \mathbf{R}_\mathrm{d} \end{pmatrix}, \tag{24}$$

$$\begin{pmatrix} \mathbf{M}_\mathrm{c}(\Delta z) \\ \mathbf{M}_+(\Delta z) \\ \mathbf{M}_-(\Delta z) \end{pmatrix} = \begin{pmatrix} \mathbf{T}_\mathrm{c} \\ \mathbf{T}_\mathrm{d} \\ \mathbf{0} \end{pmatrix}, \tag{25}$$

where $\mathbf{T}_\mathrm{c}$ is the coherent Mueller matrix transmittance. Reflectance and transmittance at the $z = 0$ and $z = \Delta z$ interfaces can be included with other boundary conditions but are not included here for simplicity.

We proceed by considering an isotropic, non-absorbing medium, so that $\mathbf{m} = \mathbf{0}$, and

$$\mathbf{s}_\mathrm{f} = \mathrm{diag}(s_{\mathrm{f},00}, s_{\mathrm{f},11}, s_{\mathrm{f},11}, s_{\mathrm{f},33}), \tag{26}$$

$$\mathbf{s}_\mathrm{b} = \mathrm{diag}(s_{\mathrm{b},00}, s_{\mathrm{b},11}, -s_{\mathrm{b},11}, s_{\mathrm{b},33}). \tag{27}$$

As a last simplification, to reduce the number of degrees of freedom of the model, we let $\mathbf{s}'_\mathrm{f} = \mathbf{s}_\mathrm{f}$ and $\mathbf{s}'_\mathrm{b} = \mathbf{s}_\mathrm{b}$. The above 12×12 matrix reduces to four 3×3 matrices:

$$\begin{pmatrix} -s_{\mathrm{f},00} - s_{\mathrm{b},00} & 0 & 0 \\ s_{\mathrm{f},jj} & -C_j & s_{\mathrm{b},jj} \\ -s_{\mathrm{b},jj} & -s_{\mathrm{b},jj} & C_j \end{pmatrix}, \tag{28}$$

with

$$C_j = s_{\mathrm{b},00} + s_{\mathrm{f},00} - s_{\mathrm{f},jj}. \tag{29}$$

The solution to Eqs. (23) through (27) is

$$T_{\mathrm{d},00} = \frac{1}{1 + s_{\mathrm{b},00}\Delta z} - T_{\mathrm{c},00}, \tag{30}$$

$$T_{\mathrm{c},jj} = T_{\mathrm{c},00} = \exp[-(s_{\mathrm{f},00} + s_{\mathrm{b},00})\Delta z], \tag{31}$$

$$\begin{aligned} T_{\mathrm{d},jj} \quad = \quad & \cosh(S_j\Delta z) - \frac{C_j \sinh(S_j\Delta z)}{S_j} \\ & + \frac{s^2_{\mathrm{b},jj} \sinh(S_j\Delta z)}{S_j^2 \coth(S_j\Delta z) + S_j C_j} - T_{\mathrm{c},00}, \end{aligned} \tag{32}$$

$$R_{\mathrm{d},jj} = \frac{s_{\mathrm{b},jj}}{C_j + S_j \coth(S_j\Delta z)}, \tag{33}$$

where

$$S_j = \sqrt{C_j^2 - s^2_{\mathrm{b},jj}}. \tag{34}$$

As expected, the coherent stream decays exponentially with thickness (Eq. 31), with a rate given by the total scattering rate $s_{\mathrm{f},00} + s_{\mathrm{b},00}$. For small Δz, we have

$$T_{\mathrm{d},jj} \approx s_{\mathrm{f},jj}\Delta z + \frac{(\Delta z)^2}{2}\{s_{\mathrm{b},jj} + s_{\mathrm{f},jj}[s_{\mathrm{f},jj} - 2(s_{\mathrm{b},00} + s_{\mathrm{f},00})]\}. \tag{35}$$

When one measures the radiation transmitting through a material, with the detector collecting radiation within angle β, the signal contains all of the coherent beam but only a fraction f of the diffuse scatter. If the diffuse radiation were Lambertian, for example, then $f = \sin^2\beta$. Thus, we expect that we would be measuring a Mueller matrix transmittance approximately given by

$$\mathbf{T} = \mathbf{T}_\mathrm{c} + f\mathbf{T}_\mathrm{d}. \tag{36}$$

The logarithmic decomposition is diagonal with

$$L_{jj} = \log[(T_{\mathrm{c},jj} + fT_{\mathrm{d},jj})/(T_{\mathrm{c},00} + fT_{\mathrm{d},00})]. \tag{37}$$

For the $\beta = 1^\circ$, 5°, and 20° detectors and Lambertian scatter, $f = 0.00030$, 0.0076, and 0.117, respectively.

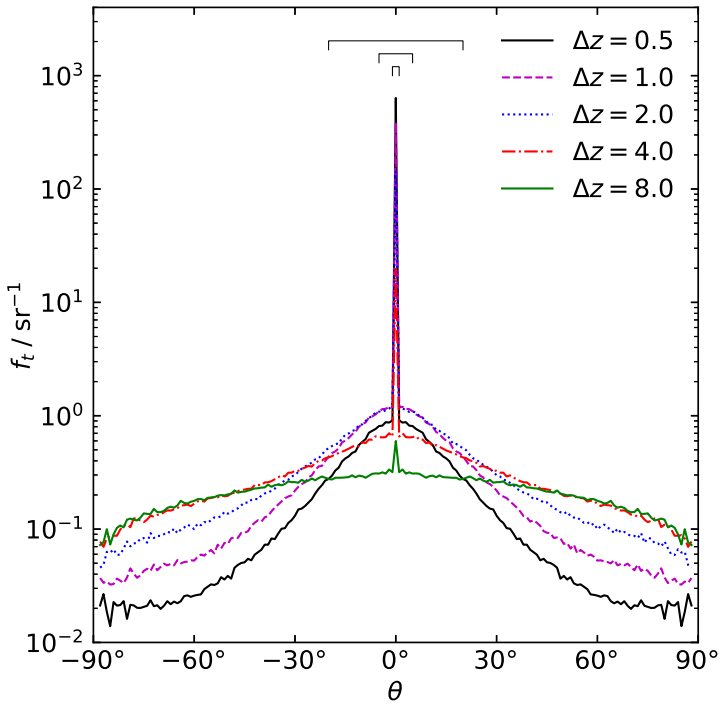

Fig. 4. The bidirectional transmittance distribution function f_t calculated using the MC method with the $D_0 = 250$ nm distribution for five different sample thicknesses. The markings at the top indicate the virtual detector collection angles used in this study.

5. Results and Discussion

Figure 4 shows the angular distribution expressed as the azimuthally-averaged, normal-incidence bidirectional transmittance distribution function f_t averaged in 1° polar angle intervals for the $D_0 = 250$ nm phase function and different thicknesses. For thin layers, most of the radiation transmits through the material unscattered, thus yielding a delta-function-like peak at zero angle. For a thin layer, the small amount of diffuse scatter at $|\theta| > 0$ is primarily due to single scattering, mimicking the phase function of the scatterers. As the thickness grows, the peak at zero angle decreases exponentially, and the diffuse scatter rises and flattens out as multiple scattering begins to dominate. At even larger thicknesses, the peak at zero angle disappears entirely and the diffuse scatter lowers as the material becomes opaque. The markings shown above the peak in Fig. 4 represent detectors spanning those used in the MC simulations. Thus, a detector which only spans ±1° is going to weigh the coherent beam much more than the diffuse scatter, compared to that which spans ±5° and ±20°.

The symbols in Fig. 5 show the MC results for the polarization-average measured transmittance (T_{00}) and the two unique and depolarizing elements of the logarithmic decomposition (L_{11} and L_{33}) for each of the three phase functions and for $\beta = 1°$, 5°, and 20°. (The curves drawn through the data are fits from the three-stream model and will be described later in this section.) The transmittance first decays exponentially at one rate and then transitions to another slower rate. The signal for a smaller detector decays with the first rate for much longer before flattening out at a lower level. For the largest detector, the behavior of the elements of the logarithmic decomposition starts out approximately quadratic and becomes linear at larger Δz. For the smaller

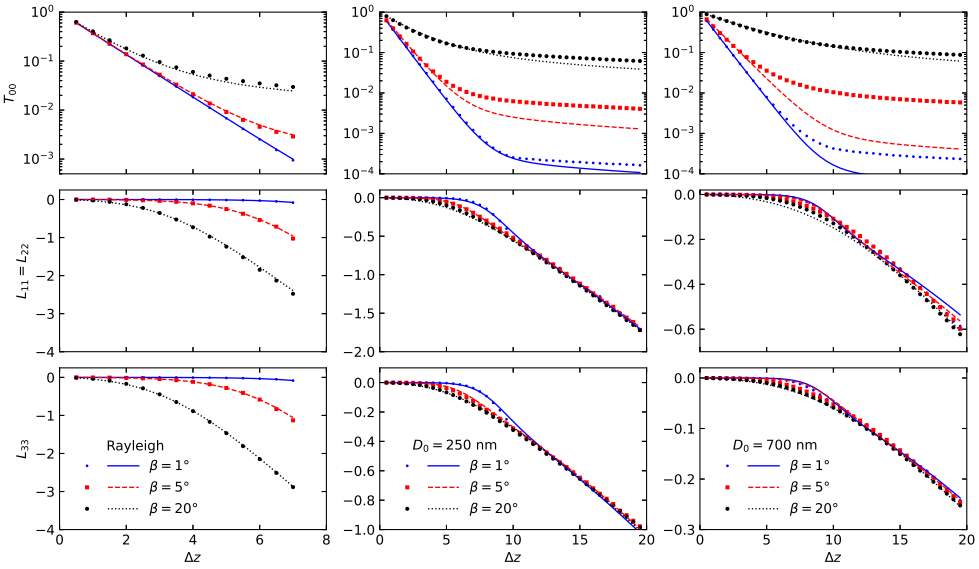

Fig. 5. The results of the MC simulations (symbols) as a function of normalized sample thickness. The top row shows the effective transmittance T_{00}. The bottom two rows show the non-zero depolarizing logarithmic decomposition elements $L_{11} = L_{22}$ and L_{33}. The phase functions are for (left) Rayleigh, (middle) $D_0 = 250$ nm, and (right) $D_0 = 700$ nm. The curves show the best fit to the three-stream model with values given in Table 1.

detectors, the depolarization remains low (L_{11} and L_{33} near zero) until the thickness when the transmittance transitions from the first decay rate to the next. The initial decay rate observed in T_{00} is due to energy being lost from the coherent beam. Since there is no depolarization in this component, L_{11} and L_{22} show little depolarization. Thus, depolarization does not occur until the diffuse scatter becomes appreciable to the the coherent beam. This transition from the coherent-dominated to the diffuse-scatter-dominated depolarization causes a bump to appear in the depolarization. That bump is most apparent when the subtended angle is small. The more quadratic behavior for large collection angles (see Figs. 9 and 10 of [10]), the lack of depolarization for small thicknesses (see Fig. 3 of [10]), and the bump (see Fig. 5 of [10]) can all be observed in the data of Charbois and Devlaminck. Non-quadratic behavior can also be observed by Gompf *et al.* [11].

It is clear from Fig. 5 that the transmittance and its polarization are dependent upon the angle subtended by the detector and that a significantly non-quadratic behavior can be observed at small thicknesses as a result of residual coherent radiation. This finding motivated our development of the three-stream model described in Sec. 4. Figure 5 shows the results of simultaneously fitting Eqs. (36) (T_{00}) and (37) (L_{11} and L_{33}) to each of the sets of MC results (that is, for each phase function and each subtended detector angle). The fitting parameters are $s_{\mathrm{b},00}$, $s_{\mathrm{b},11}$, $s_{\mathrm{b},33}$, and f. The forward scattering parameters $s_{\mathrm{f},jj}$ were set to zero and adding them did not substantially improve the results. The results for these fits are given in Table 1 and shown as curves in Fig. 5. While the results of these fits are marginal, especially for the 700 nm phase function, they show the characteristic features of the MC results.

The fits were improved substantially if we allowed $\mathbf{s}'_{\mathrm{f}} \neq \mathbf{s}_{\mathrm{f}}$ and $\mathbf{s}'_{\mathrm{b}} \neq \mathbf{s}_{\mathrm{b}} \neq \mathbf{0}$, that is, allowing scattering from the coherent stream to be different than that between the diffuse streams. The directional average for these scattering rates are different, so allowing these to differ is plausible.

Table 1. Best fit three-stream parameters shown as curves in Fig. 5.

β	$s_{b,00}$	$s_{b,11}/s_{b,00}$	$s_{b,33}/s_{b,00}$	f
Rayleigh				
1°	1.000	0.837	0.756	0.00066
5°	1.002	0.849	0.797	0.018
20°	0.992	0.744	0.588	0.109
$D_0 = 250$ nm				
1°	1.012	0.984	0.991	0.0022
5°	0.906	0.980	0.990	0.024
20°	0.474	0.928	0.963	0.398
$D_0 = 700$ nm				
1°	0.983	0.996	0.998	0.0012
5°	0.768	0.992	0.997	0.0065
20°	0.273	0.938	0.977	0.369

While the fits improved substantially, especially for the $D_0 = 700$ nm phase function, the resulting parameters were sometimes non-physical (negative or overpolarizing scattering rates), and were not necessarily unique. Note that the fits for the Rayleigh phase function are overdetermined in this 13-parameter model.

We also fit each frame (T_{00}, L_{11}, or L_{33}) in Fig. 5 to parameters needed for those data individually ($s_{f,00}$, $s_{b,00}$, and f for T_{00}; $s_{f,00}$, $s_{b,00}$, $s_{f,11}$, $s_{b,11}$, and f for L_{11}; and $s_{f,00}$, $s_{b,00}$, $s_{f,33}$, $s_{b,33}$, and f for L_{33}). In this case, $\mathbf{s}'_f = \mathbf{s}_f$ and $\mathbf{s}'_b = \mathbf{s}_b$. These results nearly identically passed through the MC results but are not shown. Charbois and Devlaminck fit their data to their fluctuation theory in this manner. That is, they did not require self-consistency between the transmittance (T_{00}) information and the polarization or between the linear (L_{11}) and circular (L_{33}) depolarization. We also are able to achieve excellent fits to all of the data of Charbois and Devlaminck in this fashion.

There is little doubt that depolarization arises from fluctuations in the Mueller matrix encountered by the various paths that radiation takes as it propagates through a material. The single-stream fluctuation theory, however, does not recognize that the optical path length experienced by transmitted radiation in a diffuse medium can be significantly greater than the thickness. Several studies have investigated the photon path length statistics for multiple scattering [20–23]. Figure 6 shows the mean path length $\langle \Lambda \rangle$ calculated from the MC method for the three phase functions and for $\beta = 20°$. The path lengths are found to deviate significantly from that of the thickness (shown as a dashed line), which represents the minimum path length needed to traverse the medium. At large Δz, the path lengths approach quadratic behavior. A fluctuation theory result may be appropriate, if one interprets the correlation length to be the scattering length and the propagation coordinate to be the actual path length. A small acceptance angle biases the collected rays toward those with shorter path lengths compared to that with a large acceptance angle.

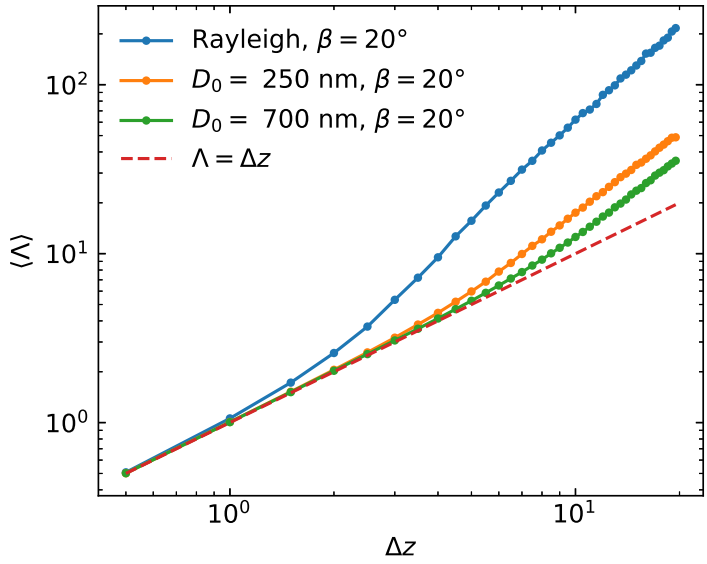

Fig. 6. Mean path length $\langle\Lambda\rangle$ of transmitted rays calculated from the MC simulations for the three phase functions and the for $\beta = 20°$ as a function of thickness Δz. The dashed line shows $\langle\Lambda\rangle = \Delta z$, corresponding to the unscattered path.

6. Conclusion

In this paper, we have provided an alternative perspective for the evolution of depolarization in diffuse media, compared to that offered by a single-stream fluctuation theory. We presented MC simulations that show that the presence of the coherent beam can strongly influence the measurement of depolarization and lead to non-quadratic behavior in the measurement. A three-stream approach captures most of the details of those simulated measurements. Future interpretations of the evolution of depolarization with sample thickness should keep in mind that scattering influences the optical path length experienced by the radiation and that it is not enough to consider the physical thickness of the material.

A. Appendix

The solution to Eq. (1) can be expressed as [19]

$$\begin{aligned}\mathbf{M}(\Delta z) &= \mathbf{I} + \int_0^{\Delta z} \mathbf{m}(z')\,\mathrm{d}z' \\ &\quad + \int_0^{\Delta z}\int_0^{z'} \mathbf{m}(z')\mathbf{m}(z'')\,\mathrm{d}z''\,\mathrm{d}z' + \cdots .\end{aligned} \tag{A.1}$$

If we let $\mathbf{m}(z) = \mathbf{m}_0 + \Delta\mathbf{m}(z)$, where $\mathbf{m}_0 = \langle\mathbf{m}(z)\rangle$ and $\langle\Delta\mathbf{m}(z)\rangle = \mathbf{0}$, and assume that $\Delta\mathbf{m}(z)$ follows a Gaussian correlation function,

$$\langle\Delta\mathbf{m}(z')\Delta\mathbf{m}(z'')\rangle = \langle\Delta\mathbf{m}^2\rangle \exp[-(z'-z'')^2/z_\mathrm{g}^2], \tag{A.2}$$

where z_g is the correlation length, we find that the average Mueller matrix is given by

$$\begin{aligned}\langle \mathbf{M}(\Delta z)\rangle &= \mathbf{I} + \mathbf{m}_0\Delta z + \frac{1}{2}\mathbf{m}_0^2(\Delta z)^2 \\ &\quad + \langle \Delta \mathbf{m}^2\rangle \frac{z_g}{2}\left\{ z_g\left[\exp\left(-\frac{(\Delta z)^2}{z_g^2}\right) - 1\right]\right. \\ &\quad \left. + \pi^{1/2}\Delta z \,\mathrm{erf}\left(\frac{\Delta z}{z_g}\right)\right\} + \cdots . \end{aligned} \tag{A.3}$$

When the fluctuations are small, the logarithmic decomposition is approximately given by

$$\begin{aligned}\mathbf{L} &= \mathbf{m}_0\Delta z \\ &\quad + \langle \Delta \mathbf{m}^2\rangle \frac{z_g}{2}\left\{ z_g\left[\exp\left(-\frac{(\Delta z)^2}{z_g^2}\right) - 1\right]\right. \\ &\quad \left. + \pi^{1/2}\Delta z \,\mathrm{erf}\left(\frac{\Delta z}{z_g}\right)\right\} + \cdots . \end{aligned} \tag{A.4}$$

When Δz is small ($\Delta z \ll z_g$),

$$\mathbf{L} = \langle \mathbf{m}\rangle \Delta z + \frac{1}{2}\langle \Delta \mathbf{m}^2\rangle (\Delta z)^2 \tag{A.5}$$

[same as Eq. (4)], and when Δz is large ($\Delta z \gg z_g$),

$$\mathbf{L} = \langle \mathbf{m}\rangle \Delta z + \frac{1}{2}\langle \Delta \mathbf{m}^2\rangle (\pi^{1/2} z_g \Delta z - z_g^2) \tag{A.6}$$

[same as Eq. (5)]. For an exponential correlation function, with correlation length z_e,

$$\langle \mathbf{m}(z')\mathbf{m}(z'')\rangle = \langle \Delta \mathbf{m}^2\rangle \exp(-|z' - z''|/z_e^2), \tag{A.7}$$

and the logarithmic decomposition is approximately given by

$$\begin{aligned}\mathbf{L} &= \mathbf{m}_0\Delta z \\ &\quad + \langle \Delta \mathbf{m}^2\rangle z_e\left\{ z_e\left[\exp\left(-\frac{\Delta z}{z_e}\right) - 1\right]\right. \\ &\quad \left. + \Delta z\right\} + \cdots . \end{aligned} \tag{A.8}$$

For small Δz, we get the same expression as Eq. (A.5), and for large Δz, we get

$$\mathbf{L} = \langle \mathbf{m}\rangle \Delta z + \langle \Delta \mathbf{m}^2\rangle (z_e \Delta z - z_e^2). \tag{A.9}$$

Disclosures. The author declares no conflicts of interest.

Acknowledgment. The author would like to thank Razvigor Ossikovski for very insightful discussions.

References

1. A. Pierangelo, A. Benali, M.-R. Antonelli, T. Novikova, P. Validire, B. Gayet, and A. D. Martino, "Ex-vivo characterization of human colon cancer by mueller polarimetric imaging," Opt. Express **19**, 1582–1593 (2011).
2. D. Bicout, C. Brosseau, A. S. Martinez, and J. M. Schmitt, "Depolarization of multiply scattered waves by spherical diffusers: Influence of the size parameter," Phys. Rev. E **49**, 1767–1770 (1994).

3. W.-N. Chen, C.-W. Chiang, and J.-B. Nee, "Lidar ratio and depolarization ratio for cirrus clouds," Appl. Opt. **41**, 6470–6476 (2002).
4. A. T. Young, "Revised depolarization corrections for atmospheric extinction," Appl. Opt. **19**, 3427–3428 (1980).
5. M. W. Williams, "Depolarization and cross polarization in ellipsometry of rough surfaces," Appl. Opt. **25**, 3616–3622 (1986).
6. W. Burns, R. Moeller, and C.-L. Chen, "Depolarization in a single-mode optical fiber," J. Light. Technol. **1**, 44–50 (1983).
7. N. Agarwal, J. Yoon, E. Garcia-Caurel, T. Novikova, J.-C. Vanel, A. Pierangelo, A. Bykov, A. Popov, I. Meglinski, and R. Ossikovski, "Spatial evolution of depolarization in homogeneous turbid media within the differential mueller matrix formalism," Opt. Lett. **40**, 5634–5637 (2015).
8. S. H. Yoo, R. Ossikovski, and E. Garcia-Caurel, "Experimental study of thickness dependence of polarization and depolarization properties of anisotropic turbid media using mueller matrix polarimetry and differential decomposition," Appl. Surf. Sci. **421** (2017).
9. H. R. Lee, T. S. H. Yoo, P. Li, C. Lotz, F. K. Groeber-Becker, S. Dembski, E. Garcia-Caurel, R. Ossikovski, and T. Novikova, "Mueller microscopy of anisotropic scattering media: theory and experiments," in *Unconventional Optical Imaging,* vol. 10677 C. Fournier, M. P. Georges, and G. Popescu, eds., International Society for Optics and Photonics (SPIE, 2018), pp. 222 – 229.
10. J. M. Charbois and V. Devlaminck, "Stochastic model for the differential mueller matrix of stationary and nonstationary turbid media," J. Opt. Soc. Am. A **33**, 2414–2424 (2016).
11. B. Gompf, M. Gill, M. Dressel, and A. Berrier, "On the depolarization in granular thin films: a mueller-matrix approach," J. Opt. Soc. Am. A **35**, 301–308 (2018).
12. R. C. Jones, "A new calculus for the treatment of optical systems. vii. properties of the n-matrices," J. Opt. Soc. Am. **38**, 671–685 (1948).
13. R. M. A. Azzam, "Propagation of partially polarized light through anisotropic media with or without depolarization: A differential 4×4 matrix calculus," J. Opt. Soc. Am. **68**, 1756–1767 (1978).
14. R. Ossikovski and A. D. Martino, "Differential mueller matrix of a depolarizing homogeneous medium and its relation to the mueller matrix logarithm," J. Opt. Soc. Am. A **32**, 343–348 (2015).
15. G. Strang, *Linear Algebra and Its Applications* (Academic Press, New York, 1980), p. 205, 2nd ed.
16. N. Ortega-Quijano and J. L. Arce-Diego, "Mueller matrix differential decomposition," Opt. Lett. **36**, 1942–1944 (2011).
17. R. Ossikovski, "Differential matrix formalism for depolarizing anisotropic media," Opt. Lett. **36**, 2330–2332 (2011).
18. R. Ossikovski and O. Arteaga, "Statistical meaning of the differential mueller matrix of depolarizing homogeneous media," Opt. Lett. **39**, 4470–4473 (2014).
19. V. Devlaminck, "Depolarizing differential mueller matrix of homogeneous media under gaussian fluctuation hypothesis," J. Opt. Soc. Am. A **32**, 1736–1743 (2015).
20. G. H. Weiss, R. Nossal, and R. F. Bonner, "Statistics of penetration depth of photons re-emitted from irradiated tissue," J. Mod. Opt. **36**, 349–359 (1989).
21. A. H. Gandjbakhche, G. H. Weiss, R. F. Bonner, and R. Nossal, "Photon path-length distributions for transmission through optically turbid slabs," Phys. Rev. E **48**, 810–818 (1993).
22. M. Dogariu and T. Asakura, "Photon pathlength distribution from polarized backscattering in random media," Opt. Eng. **35**, 2234–2239 (1996).
23. A. Y. Polishchuk, J. Dolne, F. Liu, and R. R. Alfano, "Average and most-probable photon paths in random media," Opt. Lett. **22**, 430–432 (1997).
24. T. A. Germer, "Scattering mechanism for quadratic evolution of depolarization," Opt. Lett. **45**, 483–486 (2020).
25. P. Kubelka and F. Munk, "Ein beitrag zur optik der farbanstriche," Z. Tech. Physik **12**, 593–601 (1931).
26. B. Hapke, *Theory of Reflectance and Emittance Spectroscopy* (Cambridge University, Cambridge, 1993).
27. N. Ortega-Quijano and J. L. Arce-Diego, "Mueller matrix differential decomposition for direction reversal: application to samples measured in reflection and backscattering," Opt. Express **19**, 14348–14353 (2011).